Journal of
Synchrotron Radiation

ISSN 0909-0495

Received 15 February 2009
Accepted 6 May 2009

Impact of ketone and amino on the inner shell of guanine

Quan Zhu,[a,b] Feng Wang[a]* and Elena P. Ivanova[c]

[a]Center for Molecular Simulation, Faculty of Information and Communication Technologies, Swinburne University of Technology, Hawthorn, Melbourne, Victoria 3122, Australia, [b]College of Chemical Engineering and State Key Laboratory of Biotherapy, Sichuan University, Chengdu 610065, People's Republic of China, and [c]Environment and Biotechnology Centre, Faculty of Life and Social Sciences, Swinburne University of Technology, Hawthorn, Melbourne, Victoria 3122, Australia. E-mail: fwang@swin.edu.au

Removal of the functional groups of guanine, *i.e.* ketone and amino, one by one produces model molecules of hypoxanthine, 2-aminopurine and unsubstituted purine. The impact of the ketone and amino moieties on guanine is revealed using their atomic-site-based inner-shell electronic properties and spectra. A density functional theory based model has been employed to study the model molecules. Electronic properties, such as Hirshfeld charges and inner-shell chemical shift, are found to be both site-dependent and moiety-dependent. The site-based inner-shell chemical shift of the species exhibits a simple linear correlation, although certain similarities among the model molecules regroup the species into two pairs of purine and 2-aminopurine, as well as hypoxanthine and guanine.

Keywords: guanine model molecules; inner-shell ionization spectra; Hirshfeld charge; chemical shift; condensed Fukui function.

1. Introduction

In recent years, photon-induced ionization mechanisms and dynamical processes of biological molecules have been recognized as being able to reveal further insight into damage to biological cells and tissues (Kent *et al.*, 1993; Dreuw, 2006; Magulick *et al.*, 2006). When a photoabsorption process occurs in biological systems such as living cells, it may cause certain (photobiological) effects on the system, such as direct DNA strand breaks (Yokoya *et al.*, 1999). Moreover, a large number of secondary electrons and radical cations of DNA bases generated from radiation can react with biomolecules and cause DNA strand breaks, base fragmentation and base release in dry DNA under vacuum (Cai *et al.*, 2006; Cauet *et al.*, 2006; Huels *et al.*, 2003). A combination of initial ionization and subsequent interactions and reactions will result in chromosome aberrations, mutations, cellular inactivation and finally cellular or tissue death (Gobert *et al.*, 2004; Fayard *et al.*, 2002).

As the media surrounding the molecules are very complex in real biological systems, the requirement for structural and intrinsic properties of the model molecules in the gas phase arises to understand the fundamental biological phenomena caused by radiation. Inner-shell events have attracted great attention in recent years, either experimentally or theoretically, for constituent molecules such as amino acids and nucleic bases (Plekan *et al.*, 2008; Cai *et al.*, 2005; Ptasinska *et al.*, 2008; Fujii *et al.*, 2003, 2004; Peeling *et al.*, 1978*a*,*b*; Takahata *et al.*, 2006; Saha *et al.*, 2008; Wang *et al.*, 2008). Compared with the valence shell, the inner shell contributes a major part to the total electronic energy of a molecule, and exhibits a strong screening effect on the outer neighbours which, in return, influences the active sites and bonding strength in the molecules. Furthermore, orbitals of inner-shell electrons exhibit a localized and element-dependent character, which provides clear information for correlating their ionization spectra with atomic sites in a molecule (Wang, 2005; Wang *et al.*, 2005; Saha *et al.*, 2008; Takahata *et al.*, 2006).

With the aid of synchrotron radiation sources, experimental techniques such as near-edge X-ray absorption fine-structure spectroscopy, X-ray absorption spectroscopy and X-ray photoemission spectroscopy have been used to study the inner-shell binding/excitation energy spectra of biomolecules in the gas phase (Plekan *et al.*, 2008; Cai *et al.*, 2005; Ptasinska *et al.*, 2008; Fujii *et al.*, 2003, 2004; Peeling *et al.*, 1978*a*,*b*). However, for larger biomolecules containing a number of atoms of the same element, such as nucleic bases, these experimental techniques are likely to assign the major spectral peaks, separated by a large chemical shift owing to their resolutions (Plekan *et al.*, 2008). On the other hand, inner-shell ionization processes of these biomolecules provide a major challenge to theory and many of the methods developed for

small inorganic molecules (Chong, 1995; Loos & Assfeld, 2007) are hardly applicable to biomolecules (Wang *et al.*, 2008).

The development of theory to accurately predict larger (bio)molecules has been envisaged (Tarantelli & Cederbaum, 1989; Thiel *et al.*, 2003; Nakata *et al.*, 2006; Chong *et al.*, 2004). However, even for biomolecules as large as nucleic bases, accurate prediction of the core-electron binding energies is computationally expensive, so that most of the post-Hartree–Fock (HF) methods including MP2 become inapplicable. Methods based on density functional theory (DFT) are not usually directly applicable to calculating binding energies of a molecule as Koopman's theorem does not apply to orbital energies owing to self-energies (Tu *et al.*, 2007). For small molecules, particularly inorganic molecules, Chong (1995) developed a DFT-based method for core-electron binding energies (CEBEs). In this method a CEBE can be calculated using ΔE(PW86-PW91) + C_{rel} (Chong, 1995). The second term, C_{rel}, is produced semi-empirically. Later, Loos & Assfeld (2007) adopted the Boys–Foster localization criterion to determine the hole core orbital and to obtain the C1*s* binding energy in different chemical surroundings using the PBE0/6-311++G** model (Loos & Assfeld, 2007).

For larger molecules such as DNA bases, an *ab initio* method using the fourth-order algebraic diagrammatic construction method ADC(4) (Thiel *et al.*, 2003) and one-particle Green's function has been used to interpret the X-ray photoemission spectra of thymine and adenine with a systematic correction (Plekan *et al.*, 2008; Thiel *et al.*, 2003). In our recent studies (Saha *et al.*, 2008; Wang *et al.*, 2008), a DFT model with LB94 exchange-correlation potential (van Leeuwen & Baerends, 1994) and the 'meta-Koopman theorem' (Chong, 1995) was employed in the simulation of inner-shell binding-energy spectra for DNA bases such as purine and pyrimidine bases. In these studies, the simulated inner-shell binding-energy spectra exhibit competitive accuracy to results obtained from a more computationally demanding ADC(4) model (Plekan *et al.*, 2008). More recently, the same group (Thompson *et al.*, 2009) further compared this DFT-based model on a nucleoside, cytidine, with a recently developed model of CV-B3LYP (Nakata *et al.*, 2006) and yielded a compatible accuracy. In this work, the same model is employed to study model molecules of guanine in the inner shell, in order to reveal the impact of ketone and amino moieties on the inner-shell electronic structures of guanine (Gu) and purine (Pu) through model molecules of hypoxanthine (Hx) and 2-aminopurine (Ap).

The model molecules, hypoxanthine (Hx) and 2-aminopurine (Ap), are also important building blocks of life. Hypoxanthine, a purine metabolic intermediate in living systems, also exists in transfer RNA as a minor Pu base (Stryer, 1988; Tokdemir & Nelson, 2005). 2-Aminopurine, which could form Watson–Crick base pairs with thymine (T) without disrupting the DNA double helix, is often used as a quasi-intrinsic fluorescent probe of the structure and dynamics of DNA (Su *et al.*, 2004; Vilkaitis *et al.*, 2000; Sowers *et al.*, 1986). In a study of inner-shell properties of purine bases (Wang *et al.*, 2008), guanine shows very little inheritance from its parent purine in the inner shell. As the ketone and amino moieties (C═O and $-NH_2$) on the pyrimidine (hexagon) ring of Gu may influence the C1*s* and N1*s* spectra with respect to unsubstituted Pu, questions arise. For example, would the moieties exhibit different effects on the inner-shell chemical shift? If yes, how much? Are the chemical shifts related when one moiety at a time contacts the pyrimidine ring? We attempt to reveal these insights in the present study.

2. Computational details

All geometries of the four model molecules, guanine, purine, hypoxanthine and 2-aminopurine, are fully optimized at the level of B3LYP/aug-cc-pVTZ, using the *Gaussian03* computational chemistry package (Frisch *et al.*, 2004) followed by harmonic vibrational analysis. The stable geometries have been obtained without any virtual frequencies. Based on the LB94/et-pVQZ model (van Leeuwen & Baerends, 1994; Chong *et al.*, 2004), single-point calculations employing the *ADF* (*Amsterdam Density Functional*) computational chemistry package (Baerends *et al.*, 2006) are then employed to produce the core orbital energies, orbital wavefunctions and properties. Core-shell ionization potential (IP) energies are calculated using the meta-Koopman theorem without further modification and scaling. The procedure has been detailed in our earlier study (Wang *et al.*, 2008). Molecular properties such as Hirshfeld charges (Hirshfeld, 1977), Fukui functions and dipole moments are produced next.

Partitioning of electron density according to the Hirshfeld scheme (Hirshfeld, 1977) has been widely applied in atomic charge analyses and calculations of atomic dipole moments and Fukui functions. The Hirshfeld scheme evaluates a point charge condensed on the kth atom in a molecule as (Hirshfeld, 1977; Proft *et al.*, 2002)

$$q_k = Z_k - \int w_k(\mathbf{r})\rho(\mathbf{r})\,\mathrm{d}\mathbf{r},$$

where Z_k and $w_k(\mathbf{r})$ are the nucleic charge and weight factor of the kth atom, respectively, and $\rho(\mathbf{r})$ represents the molecular electron density. The Hirshfeld charge can predict site selectivity which agrees well with experiment in most cases (Proft *et al.*, 2002), such as reactive sites, and is superior to other schemes such as the Mulliken and natural population analyses (Arulmozhiraja & Kolandaivel, 1997). As a result, the Hirshfeld charge scheme is employed in the present study.

Fukui functions can be evaluated by functional derivatives of chemical potentials with respect to the external potential. Recently, condensed Fukui functions have become the preferable choice for convenience in calculation and quasi-quantitative analysis (Sablon *et al.*, 2007; Ayers *et al.*, 2007), as the information is related to molecular orbitals and orbital relaxation. In the original formula, the condensed Fukui functions are defined as (Yang & Mortier, 1986; Parr & Yang, 1984)

Table 1
Geometric parameters of the model molecules obtained using the DFT-based B3LYP/aug-cc-pVTZ model (in Å); the shifts with respect to purine are given in the last three columns.

	Pu	Ap	†	Hx	‡	Gu	§	ΔHx(Pu)	ΔAp(Pu)	ΔGu(Pu)
N(1)—C(2)	1.340	1.352	1.345	1.359	1.364	1.366	1.371	0.019	0.012	0.026
C(2)—N(3)	1.334	1.341	1.331	1.297	1.300	1.306	1.314	−0.037	0.007	−0.028
N(3)—C(4)	1.323	1.323	1.321	1.357	1.359	1.354	1.360	0.034	0.000	0.031
C(4)—C(5)	1.406	1.405	1.392	1.390	1.393	1.390	1.398	−0.016	−0.001	−0.016
C(5)—C(6)	1.388	1.388	1.377	1.441	1.445	1.435	1.444	0.053	0.000	0.047
N(1)—C(6)	1.333	1.327	1.324	1.430	1.434	1.435	1.440	0.097	−0.006	0.102
C(5)—N(7)	1.385	1.387	1.396	1.375	1.376	1.379	1.383	−0.010	0.002	−0.006
N(7)—C(8)	1.303	1.300	1.287	1.305	1.308	1.302	1.310	0.002	−0.003	−0.001
C(8)—N(9)	1.378	1.385	1.387	1.375	1.379	1.381	1.386	−0.003	0.007	0.003
C(4)—N(9)	1.372	1.370	1.360	1.367	1.370	1.366	1.371	−0.005	−0.002	−0.006
R6¶	8.124	8.136	8.090	8.274	8.295	8.286	8.327	0.150	0.012	0.162
R5¶	6.844	6.847	6.822	6.812	6.826	6.818	6.848	−0.032	0.003	−0.026

† See Mishra *et al.* (2000). ‡ B3LYP/6-311++G(d,p) (Shukla & Leszczynski, 2000). § B3LYP/cc-pVDZ geometry (Mennucci *et al.*, 2001). ¶ Ring perimeters, see Wang *et al.* (2005).

$$f_k^+ = q_k(N+1) - q_k(N) \quad \text{for nucleophilic attack,}$$
$$f_k^- = q_k(N) - q_k(N-1) \quad \text{for electrophilic attack,}$$
$$f_k^0 = (1/2)\left[q_k(N+1) - q_k(N-1)\right] \quad \text{for radical attack.}$$

In these equations, $q_k(N+1)$, $q_k(N)$ and $q_k(N-1)$ represent charge populations on the kth atom of the $N+1$ (anion), N (neutral molecule) and $N-1$ (cation) electron systems of the same molecule, respectively. In this study, the charges are Hirshfeld charges.

3. Results and discussion

Chemical structures and nomenclature of the model molecules are shown in Fig. 1. Hx and Ap can be considered to be model molecules of Gu or derivatives of Pu; for example, Hx, which results in a C(6)═O bond replacing the C(6)—H bond in Pu. Alternatively, Hx can also be considered as being derived when the —N(2′)H_2 fragment connected at C(2) sites in Gu (Tokdemir & Nelson, 2005) is removed. On the other hand, Ap is considered as the C(2)—N(2′)H_2 fragment replacing the C(2)—H bond in Pu, or the ketone group at C(6) in Gu is removed, as shown in Fig. 1.

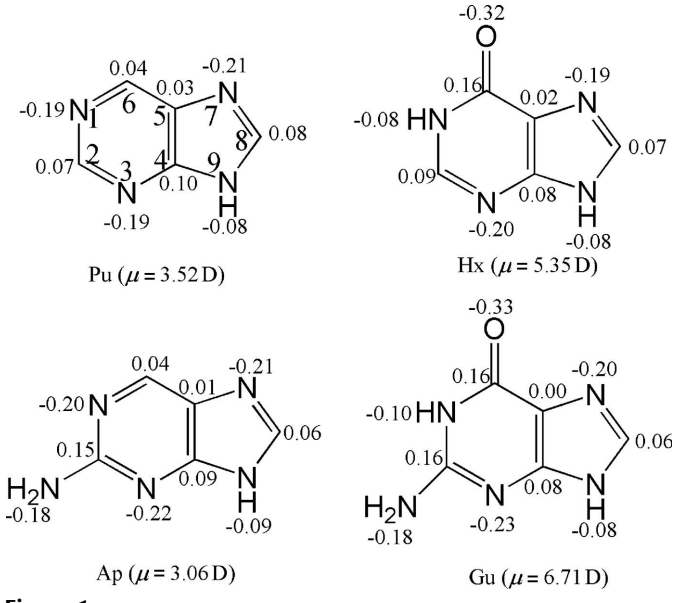

Figure 1
Structures, numbering and dipole moments of model molecules of purine (Pu), hypoxanthine (Hx), 2-aminopurine (Ap) and guanine (Gu). Hirshfeld charges are labelled on the atomic sites of the structure. The dipole moment of Gu is given by 6.26 D based on the MP2/aug-cc-pVDZ model (Choi & Miller, 2006).

It has been demonstrated that the sp^3-hybridized N atom in the amino moiety (NH_2) of guanine leads to the non-planar pyramidalization of the Gu molecular structure (Jones *et al.*, 2006; Shukla & Leszczynski, 2007; Hobza & Sponer, 1999; Sponer & Hobza, 1994). The non-planar structure in Gu is more pronounced compared with that of adenine (Jones *et al.*, 2006; Downton & Wang, 2006). The non-planar geometries of Gu and Ap possess a C_1 symmetry, whereas the planar Pu and Hx possess a *Cs* point-group symmetry. The ground electronic states of all the model molecules are closed shells with doubly occupied orbitals.

Geometric structures of the model molecules are reported in Table 1. Bond lengths in the purine ring of the model molecules are compared with results from the literature using different models (Shukla & Leszczynski, 2000; Mishra *et al.*, 2000; Mennucci *et al.*, 2001). The last three columns of this table provide deviations of the bond lengths in each molecule from those of the unsubstituted purine as references. Closer geometric similarities between the Ap and Pu pair than those between the Hx and Gu pair are seen, as the ΔAp(Pu) exhibits smaller discrepancies in bond lengths than the ΔHx(Pu) and ΔGu(Pu). Such trends are also seen in the ring perimeters of the pyrimidine (hexagon, R6) and imidazole (pentagon, R5) rings (Wang *et al.*, 2005), as indicated in Table 1. The dipole moments of molecules with ketone, Hx and Gu, are 5.35 D and 6.71 D, respectively, considerably larger than those of Pu and Ap, 3.52 D and 3.06 D, respectively.

A recent X-ray photoemission spectroscopy (XPS) study of guanine by Ptasinska *et al.* (2008) and an even more recent core shell XPS measurement of guanine tautomers by Plekan *et al.* (2009) provided a relatively high revolution, enabling us to compare our simulation with experiment for guanine. Table 2 compares inner-shell ionization potentials (IPs) of (canonical) guanine with available theoretical and experimental results. Note that only the most recent experiment of Plekan *et al.* (2009) was carried out in the gas phase. For example, in the recent XPS study, Ptasinska *et al.* (2008) used thin DNA films on grounded substrates using silver conductive paint. An earlier XPS study was performed on the surface of Cu(110) (Furukawa *et al.*, 2007). The mean IPs in the fourth column are the simple averaged absolute values of orbital energies given by the HF/aug-cc-pVTZ and B3LYP/aug-cc-pVTZ models as suggested by Powis *et al.* (2003). The mean IPs provide estimations for larger molecules where *ab initio*

Table 2
Comparison of calculated and experimental core IPs for guanine (in eV).

Atom	LB94/et-pVQZ	CEBE/TZP†	Mean IPs‡	ADC(4)§	Expt§	Expt¶	Expt††
O(6′)	533.91	536.71	539.08	536.57	536.7	531.00–532.00	531.00 ± 0.20
N(9)	404.94	406.65	408.41	406.40	406.3	400.00	400.0 (400.400)
N(1)	404.80	406.42	408.32	406.21	406.3	400.00	400.0 (400.400)
N(2′)	404.41	406.46	407.87	406.38	406.3	400.00	400.0 (400.400)
N(3)	403.36	404.72	406.69	404.51	404.5	398.00–399.00	398.40 (399.10)
N(7)	403.02	404.53	406.48	404.61	404.5	398.00–399.00	398.40 (399.10)
C(2)	293.20	293.74	295.41	294.06	293.8	289.00	
C(6)	292.49	293.30	294.59	293.25	293.8	288.00	
C(4)	291.72	292.20	293.63	292.12	292.1	286.00–287.00	
C(8)	291.40	291.79	293.25	291.93	292.1	286.00–287.00	
C(5)	290.35	290.68	291.79	290.42	290.9	285.00	

† See Takahata *et al.* (2006). ‡ Simple mean of IPs based on the models of HF/aug-cc-pVTZ and B3LYP/aug-cc-pVTZ. § The most recent gas-phase core shell spectroscopy of guanine. See Plekan *et al.* (2009). ¶ XPS experiment. See Ptasinska *et al.* (2008). †† XPS experiment on Cu(110) with the coverage θ of 0.2 ML. See Furukawa *et al.* (2007).

methods are not practical. The *ab inito* ADC(4) results of IPs for guanine (Plekan *et al.*, 2009) are also compared in this table.

The XPS experimental results [Ptasinska *et al.* (2008), as the more recent gas-phase measurement (Plekan *et al.*, 2009) has not been fully published] exhibit environment- and technique-dependent variations of the peak positions in the C1*s*, N1*s* and O1*s* spectra of guanine. Owing to the resolution, the results provide clustered peak positions for O1*s*, N1*s* and C1*s* spectra rather than a detailed site-dependent measurement, particularly in higher energy bands such as the N1*s* spectral region of 400 eV. Fig. 2 reports the N1*s* and C1*s* spectra of (canonical) guanine simulated from the present study (dashed line) and a recent XPS (solid line) experiment of Ptasinska *et al.* (2008), together with the deconvoluted spectra based on the experimental assignment (dotted lines; Ptasinska *et al.*, 2008). In the simulation, in order to remove systematic errors such as solid-state effects and orbital relaxation effects, large energy shifts of −4.6 eV and −5.6 eV, respectively, have been applied to the N1*s* and C1*s* spectra. A full width at half-maximum (FWHM) of 0.76 eV has been employed in the Gaussian shape function. For the guanine N1*s* spectra in this figure, the present results (dashed line) achieve excellent agreement with the deconvoluted spectra (dotted line) based on the experiment data (Ptasinska *et al.*, 2008). However, C1*s* spectra of guanine agree well in the lower energy side (<287 eV) of the spectra with the experiment. At the higher energy end (>287 eV), two peaks with respect to C(2) and C(6) exhibit significant red shift, compared with the experimental data. In guanine, sites C(2) and C(6) correspond to carbon sites which are either part of the ketone moiety or the carbon atom which directly connects to the amino moiety (see Fig. 1 for the structure).

Hirshfeld charges of the model molecules are given on atomic sites of the structures in Fig. 1. As observed before (Wang *et al.*, 2008; Saha *et al.*, 2008), N and O atoms possess negative charges but C atoms are deposited with positive charges. In general, Hirshfeld charges of the N sites do not exhibit significant changes with respect to the amino moiety. For example, Q(H) values on N(1) of Pu and Ap are given by −0.19 and −0.20 a.u., respectively. However, ketone significantly reduces the negative charges on N(1) in Hx and Gu with a Q(H) of −0.08 and −0.10 a.u., respectively. Q(H) of the carbon sites, however, depends on whether or not the site directly connects with the functional groups, as seen in their IP spectra. For example, Q(H) of C(2) and C(6), which directly connects to the amino and ketone groups in the species, varies depending on the moiety attached. It is no surprise that the keto oxygen leads to an increase of positive charge condensed on C(6) in Hx and Gu, owing to its strong electronegativity with respect to its counterparts in Pu and Ap. Similar behaviour is seen with respect to the charge deposited on site C(2) for the amino group. It is noted that site C(5) is almost neutral [*i.e.* Q(H) ≃

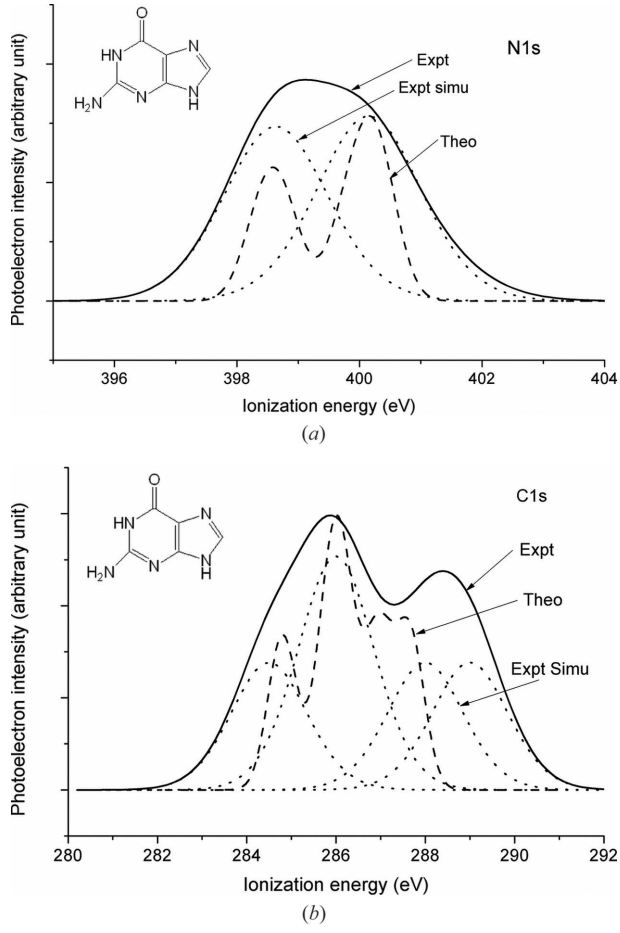

Figure 2
Comparison of N1*s* and C1*s* XPS of guanine between the experiment (solid line) and the present simulation (dashed line). The theoretical results have been constructed by Gaussian line shape of 0.76 eV FWHM and shifted the ionization energy as a whole by −4.60 eV and −5.60 eV for N1*s* and C1*s*, respectively. The experiment peaks are deconvoluted in dotted lines.

0] in all model molecules, which is also found in purine bases (Wang *et al.*, 2008).

Condensed Fukui functions for nucleophilic attack (f^+), electrophilic attack (f^-) and radical attack (f^0) have been produced and and are presented in Fig. 3. From the condensed Fukui functions, the most apparent character is that the N(9) sites in all model molecules stay almost unchanged, and the variations in the Fukui functions can be separated by N(9) which groups the negative Q(H) sites (Os and Ns) on the left-hand side from the positive Q(H) sites on the right-hand side. The f^- and f^0, which respectively represent electrophilic attack and radical attack, are more active in the oxygen and nitrogen sites as they are electron donors, whereas f^+, which attracts nucleophilic attacks, is more active in the carbon sites. The oxygen O(6′) sites of Hx and Gu exhibit large f^- values, which likely form hydrogen bonds with cytosine in DNA helix (Shukla & Leszczynski, 2007). The amino nitrogen sites, N(2′), in Ap and Gu remain inactive for these reactions, as they possess low condensed Fukui functions, whereas other N sites except for N(9) are very active, with N(3) the most active N site. It is also interesting that, for the N sites, the trend Pu > Ap > Hx > Gu almost always exists for f^+, f^- and f^0, again except for N(9). Taking the three-dimensional factor into account, the unsaturated N(3) and N(7) (imino nitrogen sites) are likely to attract electrophilic attacks by metals such as Au and Ru (Kastner *et al.*, 1981; Kumar *et al.*, 2006). As noted by a number of studies, when the condensed Fukui function is greater than 0.04 the parallel stacking is most likely the interaction when two bases are put together or a base molecule is adsorbed by a metal or non-metal surface (Sponer *et al.*, 2002; Hobza & Sponer, 1999; Seifert *et al.*, 2007; Furukawa *et al.*, 2007). When the carbon sites are more active with relatively large condensed Fukui functions f^+ and f^0, the C(2) sites in Hx and Gu and C(6) sites in Ap and Pu experience the most significant changes among the model molecules.

Fig. 4 demonstrates site-related core IPs of the model molecules and their shifts owing to attachment of the moieties; the data are given in Table 3. In unsubstituted purine, the energy ordering of the nitrogen sites is given by N(1) < N(7) < N(3) < N(9) and the carbon sites by C(5) < C(6) < C(2) < C(4)

Table 3
Calculated site-specific core IPs of the model molecules and their simple relationship (in eV).

	LB94/et-pVQZ					Fit (I)†	Fit (II)‡
Site	Pu	Gu	Ap	Hx	ΔIP(Gu–Pu)§	ΔIP (Gu–Pu)	ΔIP(Gu–Pu)
O(6′)		533.91		534.10			
N(9)	405.29	404.94	404.87	405.26	−0.35	−0.37	−0.34
N(3)	403.61	403.36	403.13	403.78	−0.25	−0.22	−0.19
N(7)	403.47	403.02	403.07	403.32	−0.45	−0.47	−0.45
N(1)	403.29	404.80	402.95	405.08	1.51	1.53	1.52
N(2′)		404.41	403.54				
C(8)	292.02	291.40	291.55	291.75	−0.62	−0.65	−0.62
C(4)	291.96	291.72	291.62	291.96	−0.24	−0.27	−0.25
C(2)	291.43	293.20	292.27	292.32	1.77	1.57	1.51
C(6)	291.05	292.49	290.77	292.70	1.44	1.43	1.43
C(5)	290.85	290.35	290.32	290.75	−0.50	−0.53	−0.49

† Fit I. $\Delta IP(Gu–Pu) = \alpha\,\Delta IP(Hx–Pu) + \beta\,\Delta IP(Ap–Pu)$ where $\alpha = 1.006$ and $\beta = 0.808$. ‡ Fit II excludes C(2) from the fitting. $\Delta IP(Gu–Pu) = \alpha\,\Delta IP(Hx–Pu) + \beta\,\Delta IP(Ap–Pu)$ where $\alpha = 0.993$ and $\beta = 0.746$. § ΔIP(Gu–Pu) is the difference of core IPs between Gu and Pu.

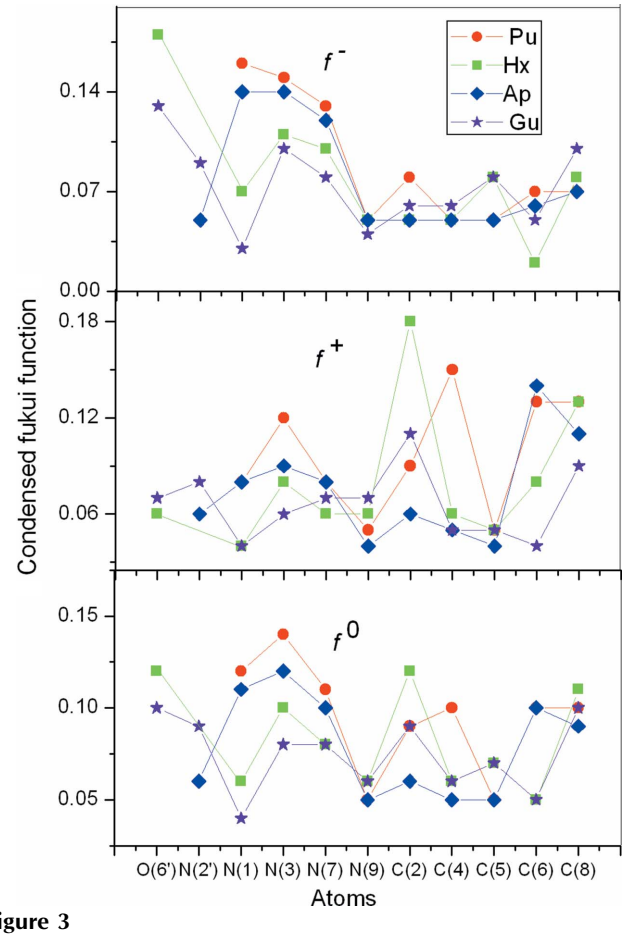

Figure 3
Condensed Fukui functions for electrophilic attack (f^-), nucleophilic attack (f^+) and radial attack (f^0) according to the Hirshfeld charges of Pu, Hx, Ap and Gu. The O*s* and N*s* sites are separated from the C*s* sites at N(9).

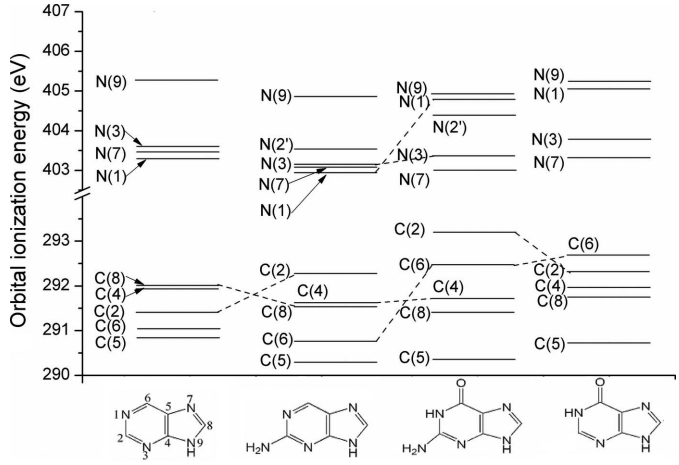

Figure 4
Core ionization energy correlation diagram of Pu, Hx, Ap and Gu.

< C(8). Addition of the amino group [N(2′)H$_2$] at the C(2) site, which forms Ap, does not alter the N ordering of Pu but N(2′) is inserted between N(3) and N(9). However, formation of an N(2′)—C(2) bond significantly increases the energy on C(2) in Ap, leading to a highest carbon energy of this site in Ap. When ketone C(6)═O replaces the C(6)—H bond in Ap, apart from the predicable C(6) energy increase in Gu which pushes up the energy of C(2), the energy of N(1) also changes significantly as the C(6)═N(1) bond in Pu and Ap becomes a single bond in Gu. As a result, the energy ordering in Gu becomes N(7) < N(3) < N(2′) < N(1) < N(9) and C(5) < C(8) < C(4) < C(6) < C(2). Finally, removal of the amino group in Gu, which gives Hx, does not affect the N site energy ordering but leads to the C(2) site energy drop to below C(6) in Hx. In these molecules, C(5) is always the lowest energy site, regardless of the attachment of amino or ketone on the purine ring, in agreement with the most recent core-shell spectrum of guanine (Plekan *et al.*, 2009).

Core ionization binding-energy spectra of the model molecules are given in Figs. 5(*a*) and 5(*b*) for the N1*s* spectra and C1*s* spectra, respectively. Although geometries of the purine ring in the model molecules do not experience significant changes when the amino and ketone moieties are connected with the purine ring, their core electronic structures, in particular their core binding-energy spectra, indicate that they are completely different molecules, regardless of whether the chemical bonding nature changes (*e.g.* Pu, Gu and Hx) or not (Pu and Ap, or Gu and Hx). However, certain similarities are seen in Gu and Hx, as well as Pu and Ap, particularly for their N1*s* spectra.

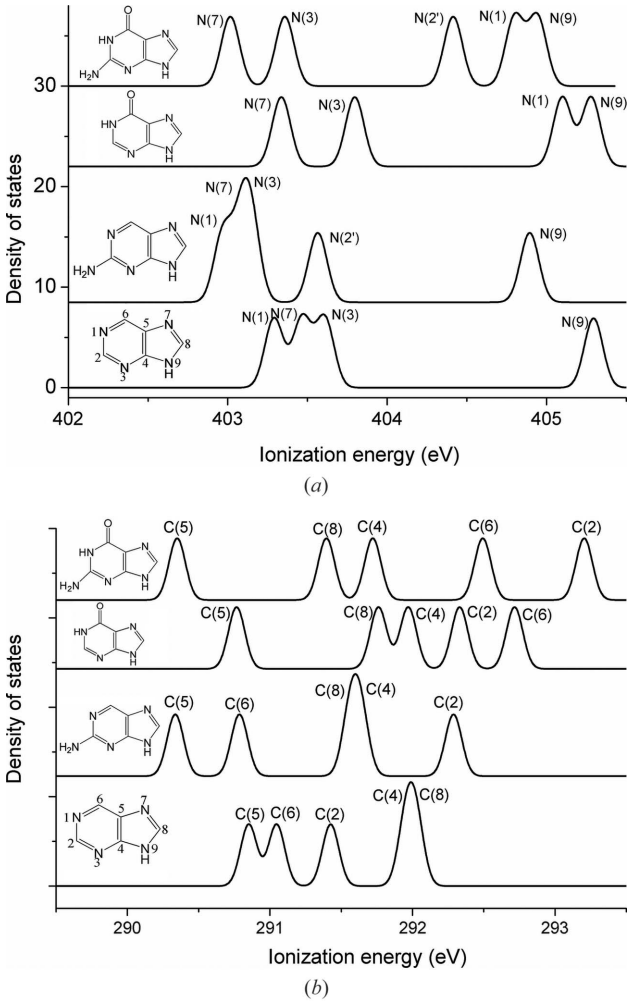

Figure 5
N1*s* ionization energy spectra (*a*) and C1*s* ionization energy spectra (*b*) of Pu, Hx, Ap and Gu.

The most apparent property of the N1*s* binding-energy spectra is the large energy gap between the imino (—N═) and the amino (—N—) nitrogen sites as indicated by Wang (2006), which is confirmed again in the core shell spectrum of guanine (Plekan *et al.*, 2009). In Pu and Ap, N(9) is the only amino N site and in Gu and Hx both N(1) and N(9) sites are amino N sites, together with the N(2′) site in Gu and Ap. As a result, the imino–amino energy gaps are over 1 eV except for Ap, whose imino–amino energy gap is given by 0.41 eV between N(2′) and N(3) rather than N(9) and N(2′). This may be caused by the conjugated chain consisting of N(1)—C(2)[N(2′)]═N(3) in Ap, which shows certain imino N character for N(2′). As a result, similarities between the Pu and Ap pair, and the Gu and Hx pair, are seen in this N1*s* spectra.

The C1*s* spectra of the molecules are even less similar, although positions of the carbon atoms in all the model molecules do not alter. However, regardless of the changes of chemical bond nature, the C1*s* spectra of all molecules are simply not the same, as found in Pu and adenine previously (Saha *et al.*, 2008). What is observed from the C1*s* spectra is (i) the C(5) site is always the first peak on the low energy end and (ii) the spectral band widths exhibit in the order Gu (2.85 eV) > Ap = Hx (1.95 eV) > Pu (1.17 eV), indicating a trend of the more functional groups on the purine ring, the larger region of the carbon spectra. Moreover, ionization energies of C(4) and C(8) are almost degenerate owing to the similar chemical surroundings in Pu and Ap, which does not happen to Hx and Gu.

Simple additions of the site-based chemical shift of Hx, Ap and Gu with respect to Pu have been observed and are listed in Table 3. It is found that certain relationship exists for the IPs of these model molecules with respect to the unsubstituted purine, such that

$$\Delta\mathrm{IP(Gu-Pu)} = \alpha\,\Delta\mathrm{IP(Hx-Pu)} + \beta\,\Delta\mathrm{IP(Ap-Pu)},$$

where parameters α and β were obtained by fitting the IPs into the above equation. The parameters α and β can be considered as the weights of the ketone and amino moieties. The fitting (Fit I) gives the (α, β) pair as (1.006, 0.808). It is noted that the IP of the C(2) site causes the largest error; if the C(2) sites are excluded from the fitting, the fitting (Fit II) gives the (α, β) pair as (0.993, 0.746). Therefore, from an energy point of view, the site-based IPs in the inner shell of Gu are dominated by the contributions of the ketone model molecule of Hx with respect to Pu, whereas the amino group makes a contribution of 80% from Ap with respect to Pu.

4. Conclusions

Varied trends of site-dependent changes such as Hirshfeld charges, condensed Fukui functions and inner-shell ionization spectra have been studied with the DFT LB94/et-pVQZ//B3LYP/aug-cc-pVTZ model. Comparison among the four model molecules, Pu, Ap, Hx and Gu, is carried out to demonstrate different effects of the keto oxygen at C(6) and the amino group at C(2) to structures and properties. It was found that Pu and Ap seem to form a pair according to the similarity of various properties, *e.g.* the condensed Fukui function, whereas Hx and Gu may form another pair.

The theoretical simulation agrees well with a recent XPS study in the gas phase (Plekan *et al.*, 2009) when the systematic errors owing to the theoretical models are removed. With comparisons among Hx, Ap, Gu and Pu it is found that the inner-shell ionization spectra of the atoms on the pyrimidine and imidazole rings change apparently in Gu and Hx owing to the bond nature changes caused by the keto oxygen. However, the amino group at the C(2) site in Ap does not lead to great changes in atomic Hirshfeld charges and inner-shell spectra for the atoms on the rings except the directly connected C(2) site, when compared with Pu. It can be concluded that the substitution through a double bond linked to the Pu rings will have greater effects on the structures and electronic properties than the substitution with a single-bond connection. In this work, the chemical shift of the inner-shell ionization energies has been a useful tool for studying the purine ring variations in hypoxanthine, 2-aminopurine and guanine.

This project is supported by a Dean's Collaborative Grant of Faculty of Information and Communication Technologies, Swinburne University of Technology. It is also supported by an award under the Merit Allocation Scheme on the APAC National Facility at the ANU. Drs S. Ptasinska and K. Prince are acknowledged for providing their most recent XPS results of guanine.

References

Arulmozhiraja, S. & Kolandaivel, P. (1997). *Mol. Phys.* **90**, 55–62.
Ayers, P. W., Proft, F. De., Borgoo, A. & Geerlings, P. (2007). *J. Chem. Phys.* **126**, 224107.
Baerends, E. J. *et al.* (2006). *ADF2006.01*. SCM, Theoretical Chemistry, Vrije Universiteit, Amsterdam, The Netherlands.
Cai, Z., Cloutier, P., Hunting, D. & Sanche, L. (2005). *J. Phys. Chem. B*, **109**, 4796–4800.
Cai, Z., Dextraze, M. E., Cloutier, P., Hunting, D. & Sanche, L. (2006). *J. Chem. Phys.* **124**, 024705.
Cauet, E., Dehareng, D. & Lievin, J. (2006). *J. Phys. Chem. A*, **110**, 9200–9211.
Choi, M. Y. & Miller, R. E. (2006). *J. Am. Chem. Soc.* **128**, 7320–7328.
Chong, D. P. (1995). *J. Chem. Phys.* **103**, 1842–1845.
Chong, D. P., Lenthe, E., van Gisbergen, S. J. A. & Baerends, E. J. (2004). *J. Comput. Chem.* **25**, 1030–1036.
Downton, M. T. & Wang, F. (2006). *Mol. Simulat.* **32**, 667–673.
Dreuw, A. (2006). *Chem. Phys. Chem.* **7**, 2259–2274.
Fayard, B. *et al.* (2002). *Radiat. Res.* **157**, 128–140.
Frisch, M. J. *et al.* (2004). *Gaussian03*, revision D.01. Gaussian Inc., Wallingford, CT, USA.
Fujii, K., Akamatsu, K., Muramatsu, Y. & Yokoya, A. (2003). *Nucl. Instrum. Methods Phys. Res. B*, **199**, 249–254.
Fujii, K., Akamatsu, K. & Tokoya, A. (2004). *J. Phys. Chem. B*, **108**, 8031–8035.
Furukawa, M., Yamada, T., Katano, S., Kawai, M., Ogasawara, H. & Nilsson, A. (2007). *Surf. Sci.* **601**, 5433–5440.
Gobert, F. N., Lamoureux, M., Herve du Penhoat, M. A., Ricoul, M., Boissiere, A., Touati, A., Abel, F., Politis, M. F., Fayard, B., Guigner, J. M., Martins, L., Testard, I., Sabatier, L. & Chetioui, A. (2004). *Int. J. Radiat. Biol.* **80**, 135–145.
Hirshfeld, F. L. (1977). *Theor. Chim. Acta*, **44**, 129–138.
Hobza, P. & Sponer, J. (1999). *Chem. Rev.* **99**, 3247–3276.
Huels, M. A., Boudaiffa, B., Cloutier, P., Hunting, D. & Sanche, L. (2003). *J. Am. Chem. Soc.* **125**, 4467–4477.
Jones, D. B., Wang, F., Brunger, M. J. & Winkler, D. A. (2006). *Biophys. Chem.* **121**, 105–120.
Kastner, M. E., Coffey, K. F., Clarke, M. J., Edmonds, S. E. & Eriks, K. (1981). *J. Am. Chem. Soc.* **103**, 5747–5752.
Kent, C. R. H., Edwards, S. M. & McMillan, T. J. (1993). *Int. J. Radiat. Biol.* **63**, 1–5.
Kumar, A., Mishra, P. C. & Suhai, S. (2006). *J. Phys. Chem. A*, **110**, 7719–7727.
Leeuwen, R. van & Baerends, E. J. (1994). *Phys. Rev. A*, **49**, 2421–2431.
Loos, P. F. & Assfeld, X. (2007). *Int. J. Quant. Chem.* **107**, 2243–2252.
Magulick, J., Beerbom, M. M. & Schlaf, R. (2006). *J. Phys. Chem. B*, **110**, 15973–15981.
Mennucci, B., Toniolo, A. & Tomasi, J. (2001). *J. Phys. Chem. A*, **105**, 7126–7134.
Mishra, S. K., Shukla, M. K. & Mishra, P. C. (2000). *Spectrochim. Acta A*, **56**, 1355–1384.
Nakata, A., Imamura, Y., Otsuka, T. & Nakai, H. (2006). *J. Chem. Phys.* **124**, 094105.
Parr, R. G. & Yang, W. (1984). *J. Am. Chem. Soc.* **106**, 4049–4050.
Peeling, J., Hruska, F. E. & McIntyre, N. S. (1978*a*). *Can. J. Chem.* **56**, 1555–1561.
Peeling, J., Hruska, F. E., McKinnon, D. M., Chauhan, M. S. & McIntyre, N. S. (1978*b*). *Can. J. Chem.* **56**, 2405–2411.
Plekan, O., Feyer, V., Richter, R., Coreno, M., de Simone, M., Prince, K. C., Trofimov, A. B., Gromov, E. V., Zaytseva, I. L. & Schirmer, J. (2008). *Chem. Phys.* **347**, 360–375.
Plekan, O., Feyer, V., Richter, R., Coreno, M., Valla-llosera, G., Prince, K. C., Trofimov, A. B., Zaytseva, I. L., Moskovskaya, T. E., Gromov, E. V. & Schirmer, J. (2009). *J. Phys. Chem. A*. Submitted.
Powis, I., Rennie, E. E., Hergenhahn, U., Kugeler, O. & Bussy-Socrate, R. (2003). *J. Phys. Chem. A*, **107**, 25–34.
Proft, F. D., Van Alsenoy, C., Peeters, A., Langenaeker, W. & Geerlings, P. (2002). *J. Comput. Chem.* **23**, 1198–1209.
Ptasinska, S., Stypczynska, A., Nixon, T., Mason, N. J., Klyachko, D. V. & Sanche, L. (2008). *J. Chem. Phys.* **129**, 065102.
Sablon, N., De Proft, F., Ayers, P. W. & Geerlings, P. (2007). *J. Chem. Phys.* **126**, 224108.
Saha, S., Wang, F., MacNaughton, J. B., Moewes, A. & Chong, D. P. (2008). *J. Synchrotron Rad.* **15**, 151–157.
Seifert, S., Gavrila, G. N., Zahn, D. R. T. & Braun, W. (2007). *Surf. Sci.* **601**, 2291–2296.
Shukla, M. K. & Leszczynski, J. (2000). *J. Mol. Struct.* **529**, 99–112.
Shukla, M. K. & Leszczynski, J. (2007). *J. Biomol. Struct. Dynam.* **25**, 93–118.
Sowers, L. C., Fazakerley, G. V., Eritja, R., Kaplan, B. E. & Goodman, M. F. (1986). *Proc. Natl. Acad. Sci. USA*, **83**, 5434–5438.
Sponer, J. & Hobza, P. (1994). *J. Phys. Chem.* **98**, 3161–3164.
Sponer, J., Leszczynski, J. & Hobza, P. (2002). *Biopolymers*, **61**, 3–31.
Stryer, L. (1988). *Biochemistry*, 3rd ed. New York: Freeman.
Su, T. J., Connolly, B. A., Darlington, C., Mallin, R. & Dryden, D. T. F. (2004). *Nucleic Acids Res.* **32**, 2223–2230.
Takahata, Y., Okamoto, A. K. & Chong, D. P. (2006). *Int. J. Quant. Chem.* **106**, 2581–2586.
Tarantelli, A. & Cederbaum, L. S. (1989). *Phys. Rev. A*, **39**, 1656–1664.

Thiel, A., Schirmer, J. & Koppel, H. (2003). *J. Chem. Phys.* **119**, 2088–2101.
Thompson, A., Saha, S., Wang, F., Tsuchimochi, T., Nakata, A., Imamura, Y. & Nakai, H. (2009). *Jpn Bull. Chem. Soc.* **82**, 187–195.
Tokdemir, S. & Nelson, W. H. (2005). *J. Phys. Chem. A*, **109**, 8732–8744.
Tu, G., Carravetta, V., Vahtras, O. & Agren, H. (2007). *J. Chem. Phys.* **127**, 174110–174111.
Vilkaitis, G., Dong, A., Weinhold, E., Cheng, X. & Klimasauskas, S. (2000). *J. Biol. Chem.* **275**, 38722–38730.
Wang, F. (2005). *J. Mol. Struct.* **728**, 31–42.
Wang, F. (2006). *Macro Nano Lett.* **1**, 23–24.
Wang, F., Downton, T. & Kidwani, N. (2005). *J. Theor. Comput. Chem.* **4**, 247–264.
Wang, F., Zhu, Q. & Ivanova, E. (2008). *J. Synchrotron Rad.* **15**, 624–631.
Yang, W. & Mortier, W. J. (1986). *J. Am. Chem. Soc.* **108**, 5708–5711.
Yokoya, A., Watanabe, R. & Hara, T. (1999). *J. Radiat. Res.* **40**, 145–158.